



# An alternative framework for E-model inflation in supergravity

Constantinos Pallis<sup>a</sup>

Laboratory of Physics, Faculty of Engineering, Aristotle University of Thessaloniki, 541 24 Thessaloniki, Greece

Received: 6 April 2022 / Accepted: 30 April 2022 / Published online: 14 May 2022  
© The Author(s) 2022

**Abstract** We present novel realizations of E-model inflation within Supergravity which are largely associated with the existence of a pole of order one in the kinetic term of the (gauge-singlet) inflaton superfield. This pole arises due to the selected logarithmic Kähler potentials  $K_1$  and  $\tilde{K}_1$ , which parameterize the same hyperbolic manifold with scalar curvature  $\mathcal{R}_K = -2/N$ , where  $(-N) < 0$  is the coefficient of a logarithmic term. The associated superpotential  $W$  exhibits the same  $R$  charge with the inflaton-accompanying superfield and includes all the allowed renormalizable terms. For  $K = K_1$ , inflation can be attained for  $N = 2$  at the cost of some tuning regarding the coefficients of the  $W$  terms and predicts a tensor-to-scalar ratio  $r$  at the level of 0.001. The tuning can be totally eluded for  $K = \tilde{K}_1$ , which allows for quadratic- and quartic-like models with  $N$  values increasing with  $r$  and spectral index  $n_s$  close or even equal to its present central observational value.

## 1 Introduction

It is well-known [1–7] that the presence of a pole in the kinetic term of the inflaton gives rise to inflationary models collectively named  $\alpha$ -attractors [8–17]. These models can be classified [12–18] into *E-Model Inflation* (EMI) [10] (or  $\alpha$ -Starobinsky model [9]) and *T-Model Inflation* (TMI) [19], depending on the form of the inflationary potential,  $V_\alpha$ , expressed in terms of the canonically normalized inflaton  $\hat{\phi}$ . Namely,  $V_\alpha$  can be defined as follows

$$V_\alpha = \begin{cases} V_E \left( 1 - e^{-\sqrt{2/N}\hat{\phi}} \right) & \text{for EMI,} \\ V_T \left( \tanh \left( \hat{\phi}/\sqrt{2N} \right) \right) & \text{for TMI,} \end{cases} \quad (1)$$

where  $N > 0$  and  $V_{E,T} = V_{E,T}(\phi)$  can be polynomial functions of the initial (non-canonical) inflaton  $\phi$ . Given that the relation between  $\phi$  and  $\hat{\phi}$  for a kinetic pole of order

two is  $\phi \sim \tanh \hat{\phi}$ , the form for  $V_T$  in (1) can be easily achieved replacing just  $\phi$  into a simple power-law potential  $V_T = V_T(\phi)$  [19]. To process similarly EMI, one would expect, that the  $\phi - \hat{\phi}$  relation would be

$$\phi = 1 - e^{-\sqrt{2/N}\hat{\phi}}. \quad (2)$$

Up-to-now, to our knowledge, the unity is omitted from the relation above and so, the attainment of EMI is less straightforward than the one of TMI— see, e.g., Ref. [17]. We below investigate the ramifications generated by the inclusion of unity in (2) within *Supergravity* (SUGRA).

In the latter context, the achievement of  $V_\alpha$  from the F-term SUGRA potential,  $V_F$ , depends on both the superpotential,  $W$ , and the Kähler potential,  $K$ , governing the singular kinetic mixing in the inflaton sector. Both  $\alpha$ -attractor models are widely connected with the hyperbolic Kähler geometry of the Poincaré disk [20] or the no-scale SUGRA [9, 11, 15]— for alternative geometries see Refs. [21–24]. These schemes, however, do not produce the  $\phi - \hat{\phi}$  relation in (2) and so, a special selection of  $W$  is required for the attainment of EMI, invoking motivations from the string theory [9, 11] or the superconformal formulation of SUGRA [10, 12–14].

Another difficulty involved in modelling E- and T-model inflation is relied on the fact that the pole appearing in the inflaton kinetic term is generically expected to emerge also in  $V_F$ . The successful implementation of inflation, however, is smoothen eliminating the pole from  $V_F$ . This aim can be accomplished [4, 5] by two alternative strategies:

- Adjusting  $W$  and constraining the curvature of the Kähler manifold, so that the pole is removed from  $V_F$  thanks to cancellations [4, 5, 8, 9] which introduce some tuning, though.
- Adopting a more structured  $K$  which yields the usual kinetic terms but remains invisible from  $V_F$  [4, 5, 12–14]. In a such case, any tuning on the  $W$  parameters can be eluded.

<sup>a</sup>e-mail: kpallis@gen.auth.gr (corresponding author)

Taking into account the above guidelines, we here establish a novel realization of EMI, tied to a simple, generic and renormalizable  $W$ , consistent with an  $R$  symmetry. This becomes possible thanks to the modified hyperbolic geometry of the internal space, which displays a pole of order one placed far away from the origin – cf. Refs. [11–14]. In a such case, (2) is naturally generated – see Sect. 3.1 – and so, EMI can be automatically processed as is done for TMI. To be more specific, we justify in the following the super- and Kähler potentials,  $W = W(z^\alpha)$  and  $K = K(z^\alpha, z^{*\bar{\alpha}})$  respectively, adopted in our proposal

Given that EMI is of chaotic type, we follow the systematic approach of Ref. [25] which bases the implementation of chaotic inflation within SUGRA on the introduction of two chiral gauge-singlet superfields, the inflaton  $z^1 = \Phi$ , and the “stabilizer” or Goldstino  $z^2 = S$ . Placing  $S$  at the origin during EMI, the derivation and the boundedness of the inflationary potential is greatly facilitated. The coexistence of  $S$  and  $\Phi$  in  $W$  can be further constrained by invoking an  $R$  symmetry under which  $S$  and  $W$  are equally charged whereas  $\Phi$  is uncharged. Contrary to others options [16,17], where a monomial  $W$  is selected, we here adopt the most general renormalizable  $W$ , i.e.,

$$W = S \left( \lambda_1 \Phi + \lambda_2 \Phi^2 - M^2 \right) \tag{3}$$

where  $\lambda_1, \lambda_2$  and  $M$  are free parameters. As we see below, thanks to the general form of  $W$  the resulting potential interpolates between the quadratic and the quartic one causing a variation to the resulting inflationary observables.

As regards  $K$ , this includes two terms:

- (a)  $K_2$  which parameterizes the compact manifold  $SU(2)/U(1)$  and assures the stability of  $S$  with respect to (w.r.t) its perturbations during EMI [26,27]

$$K_2 = N_S \ln \left( 1 + |S|^2/N_S \right) \text{ with } 0 < N_S < 6. \tag{4}$$

- (b) One of the following  $K$ 's,  $K_1$  or  $\tilde{K}_1$ , which yields the desired pole in the kinetic term of  $\Phi$  and share the same geometry. Namely,

$$K_1 = -N \ln \left( 1 - (\Phi + \Phi^*)/2 \right), \tag{5a}$$

$$\tilde{K}_1 = -N \ln \frac{(1 - \Phi/2 - \Phi^*/2)}{(1 - \Phi)^{1/2}(1 - \Phi^*)^{1/2}}, \tag{5b}$$

with  $\text{Re}\Phi < 1$  and  $N > 0$ . The placement of the singularity at unity is crucial in order to obtain the desired  $\phi - \hat{\phi}$  relation in (2). Moreover, these  $K$ 's admit a well-behaved expansion for low  $\Phi$  values. On the other hand, any connection with no-scale SUGRA [9,15] is lost.

According the aforementioned discussion, related to the elimination the pole from  $V_F$ , we can define two versions of EMI based on the  $K$ 's above:

- (a)  $\delta E$  Model ( $\delta\text{EM}$ ) in which we constrain  $N = 2$  in (5a) and tune

$$r_{21} = -\lambda_2/\lambda_1 \simeq 1 + \delta_{21} \text{ and } M \ll 1 \tag{6}$$

in (3) such that the denominator including the pole in  $V_E$  is (almost) cancelled out. Therefore,  $\delta\text{EM}$  is relied on

$$K_{12} = K_2 + K_1, \tag{7}$$

and yields results similar to the models in Refs. [8,15] which identify the inflaton with matter-like superfield.

- (b)  $E$  Model 2 (EM2) and  $E$  Model 4 (EM4) which employ

$$\tilde{K}_{12} = K_2 + \tilde{K}_1 \tag{8}$$

with free parameters  $N, \lambda_1, \lambda_2$  and  $M$  and their discrimination depends on which of the two  $\phi$ -dependent terms in Eq. (3) dominates. Obviously, for  $M \simeq 0$  and  $\lambda_2 = 0$  or  $\lambda_1 = 0$ , EM2 or EM4 coincides with the quadratic or quartic EMI respectively [10,18]. More specifically, EM2 with  $N = 3$  yields the potential of the Starobinsky model [28].

The rest of the paper is organized as follows: In Sect. 2 we describe the geometric structure of  $K_1$  and  $\tilde{K}_1$ . Then, in Sect. 3 we describe our inflationary setting and in Sect. 4 our models are confronted with observations. Our conclusions are summarized in Sect. 5. Throughout, the complex scalar components of the various superfields are denoted by the same superfield symbol, charge conjugation is denoted by a star (\*) – e.g.,  $|z|^2 = zz^*$  – the symbol  $\dot{z}$  as subscript denotes derivation with respect to (w.r.t)  $z$ , and we use units where the reduced Planck scale  $m_P = 2.44 \cdot 10^{18}$  GeV is equal to unity.

## 2 Geometry of the Kähler potentials

At a first glance, both  $K_1$  and  $\tilde{K}_1$  are invariant under the transformation  $\Phi \rightarrow \Phi^*$ , whereas  $K_1$  is in addition invariant under the non-holomorphic replacement

$$\Phi \rightarrow \Phi + it \text{ with } t \in \mathbb{R}. \tag{9}$$

However, to investigate deeper the symmetries of the  $\Phi - \Phi^*$  space and compare it with the geometry of similar models in Refs. [12,13], we determine its riemannian metric

$$ds_K^2 = K_{\Phi\Phi^*} d\Phi d\Phi^* = \frac{N}{4} \frac{d\Phi d\Phi^*}{(1 - (\Phi + \Phi^*)/2)^2} \tag{10a}$$

and the scalar curvature,

$$\mathcal{R}_K = -K^{\Phi\Phi^*} \partial_\Phi \partial_{\Phi^*} \ln(K_{\Phi\Phi^*}) = -\frac{2}{N}. \tag{10b}$$

As in the cases of Refs. [9, 12, 13] the internal space is also hyperbolic. On the other hand,  $ds_K^2$  in (10a) remains invariant under the transformation

$$\frac{\Phi}{2} \rightarrow \frac{a\Phi/2 + b}{c\Phi/2 + d}, \tag{11a}$$

with  $a, b, c, d \in \mathbb{C}$  and  $ab - cd \neq 0$ , provided that

$$b = 0, c = 2a, d = -a \text{ and } |a|^2 = 1. \tag{11b}$$

These restrictions signal a different geometry from that of Refs. [9, 12, 13]. Indeed, the matrix  $\mathbf{M}$  representing the transformation in Eqs. (11a) and (11b) has the form

$$\mathbf{M} = a \begin{pmatrix} 1 & 0 \\ 2 & -1 \end{pmatrix} \text{ with } |\det \mathbf{M}|^2 = 1 \tag{12}$$

and can be considered as an element of the set of the conjugate anti-symplectic matrices satisfying the relation

$$\mathbf{M}^\dagger \mathbf{E} \mathbf{M} = -\mathbf{E} \text{ with } \mathbf{E} = \begin{pmatrix} 0 & 1 \\ -1 & 0 \end{pmatrix} \tag{13}$$

a nonsingular antisymmetric metric-like matrix. The set of the matrices  $\mathbf{M}$  does not have a group structure – e.g., the identity does not belong to it. However, any matrix  $\mathbf{M}$  can be expressed as the product of a conjugate symplectic matrix  $\mathbf{S}$  times a fixed conjugate anti-symplectic one, such as the Pauli matrix  $\sigma_3$ . I.e.,

$$\mathbf{M} = \mathbf{S} \sigma_3 \text{ with } \sigma_3 = \text{diag}(1, -1). \tag{14}$$

It can be shown [29] that  $\mathbf{S} \in U(1, 1)$  which is a Lie subgroup of the Möbius group, i.e., the projective general linear transformation group  $PGL(2, \mathbb{C})$ .

Under the transformation in Eqs. (11a) and (11b),  $K_1$  in Eq. (5a) is transformed as

$$K_1 \rightarrow K_1 + \Lambda + \Lambda^* \text{ with } \Lambda = N \ln(1 - \Phi), \tag{15}$$

whereas  $\tilde{K}_1$  in Eq. (5b) remains precisely invariant, as can be proven, if we take into account that

$$\tilde{K}_1 = K_1 - \Lambda/2 - \Lambda^*/2. \tag{16}$$

Note that the corresponding model in Refs. [12, 13] does not enjoy a similar invariance under the  $SU(1, 1)/U(1)$  transformations. To compare further our framework with that, we introduce the “canonically normalized” superfield  $X$  (or the Killing–adapted coordinates) via the relation

$$\Phi = 1 - e^{-\sqrt{2/N}X}. \tag{17}$$

Inserting it in Eq. (5b),  $\tilde{K}_1$  can be brought into the form

$$\tilde{K}_1 = -N \ln \cosh \frac{X - X^*}{\sqrt{2N}}, \tag{18}$$

which coincides with the corresponding expression in  $SU(1, 1)/U(1)$  geometry [12, 13] despite the fact that Eq. (17) is different. From this result, we conclude that  $\tilde{K}_1$  is invariant under the shift symmetry

$$X \rightarrow X + A \text{ with } A \in \mathbb{R} \tag{19}$$

which is different from that enjoyed by  $K_1$  in Eq. (9). The last equation demonstrates the independence of  $\tilde{K}_1$  from the canonically normalized inflaton which can be identified as the real part of  $X$ .

### 3 Inflationary set-up

The (Einstein frame) action within SUGRA for the superfields  $z^\alpha$ 's – with  $\Phi$  ( $\alpha = 1$ ) and  $S$  ( $\alpha = 2$ ) – can be written as

$$\mathbf{S} = \int d^4x \sqrt{-g} \left( -\frac{1}{2} \mathcal{R} + K_{\alpha\bar{\beta}} g^{\mu\nu} \partial_\mu z^\alpha \partial_\nu z^{*\bar{\beta}} - V_F \right), \tag{20a}$$

where  $\mathcal{R}$  is the space-time Ricci scalar curvature,  $g$  is the determinant of the background Friedmann–Robertson–Walker metric,  $g^{\mu\nu}$  with signature  $(+, -, -, -)$  and summation is taken over the scalar fields  $z^\alpha$ . Also,

$$K_{\alpha\bar{\beta}} = K_{z^\alpha z^{*\bar{\beta}}} \text{ and } K^{\alpha\bar{\beta}} K_{\bar{\beta}\gamma} = \delta_\gamma^\alpha. \tag{20b}$$

The F-term SUGRA potential  $V_F$  is given by

$$V_F = e^K \left( K^{\alpha\bar{\beta}} (D_\alpha W)(D_{\bar{\beta}}^* W^*) - 3|W|^2 \right), \tag{20c}$$

where  $D_\alpha W = W_{,z^\alpha} + K_{,z^\alpha} W$ . In our analysis we use  $W$  in Eq. (3) and the  $K$ 's defined in Eqs. ((5a) and (5b)). We below, in Sect. 3.1, determine the canonically normalized fields involved in our setting, derive the inflationary potential in Sect. 3.2, find the SUSY vacuum in Sect. 3.3 and check the stability of the inflationary path in Sect. 3.4.

#### 3.1 Canonically normalized fields

The inflationary track is determined by the constraints

$$\langle S \rangle_I = \langle \Phi - \Phi^* \rangle_I = 0, \text{ or } \langle s \rangle_I = \langle \bar{s} \rangle_I = \langle \theta \rangle_I = 0 \tag{21}$$

if we express  $\Phi$  and  $S$  according to the parametrization

$$\Phi = \phi e^{i\theta} \text{ and } S = (s + i\bar{s})/\sqrt{2}. \tag{22}$$

Here the symbol “ $\langle Q \rangle_I$ ” denotes the value of a quantity  $Q$  during EMI. The canonically (hatted) normalized fields are defined as follows

$$\langle K_{\alpha\bar{\beta}} \rangle_I \dot{z}^\alpha \dot{z}^{\bar{\beta}} \simeq \frac{1}{2} \left( \dot{\hat{\phi}}^2 + \dot{\hat{\theta}}^2 + \dot{\hat{s}}^2 + \dot{\hat{\bar{s}}}^2 \right), \tag{23}$$

where the dot denotes derivation w.r.t the cosmic time,  $t$ . Taking into account Eqs. (5a) and (5b), we obtain the diagonal Kähler metric

$$\langle K_{\alpha\bar{\beta}} \rangle = \text{diag} (K_{1\Phi\Phi^*}, K_{2SS^*}), \tag{24}$$

where its elements along the inflationary path in Eq. (21) read

$$\langle K_{1\Phi\Phi^*} \rangle_I = N/4 f_p^2 \text{ with } f_p = 1 - \phi \text{ and } \langle K_{2SS^*} \rangle_I = 1. \tag{25}$$

From the first of the relations above we infer that the kinetic term of  $\phi$  exhibits a pole of order one at  $\phi = 1$ . The  $\phi$  dependent part of the left-hand side of Eq. (23) is written as

$$\langle K_{\Phi\Phi^*} \rangle_I |\dot{\Phi}|^2 = \langle K_{\Phi\Phi^*} \rangle_I \left( \dot{\phi}^2 + \phi^2 \dot{\theta}^2 \right). \tag{26}$$

Comparing the last expression with Eq. (23), in view of Eq. (25), we deduce

$$d\hat{\phi}/d\phi = J = \sqrt{N/2} f_p^{-1} \text{ and } \hat{\theta} = J\phi\theta. \tag{27}$$

Integrating Eq. (27) we can identify  $\hat{\phi}$  in terms of  $\phi$ , as follows

$$\hat{\phi} = -\sqrt{N/2} \ln(1 - \phi) \Rightarrow \phi = 1 - e^{-\sqrt{2/N}\hat{\phi}}, \tag{28}$$

which is the advertised relation in Eq. (2). We remark that  $\hat{\phi}$  gets increased from 0 to  $6.5\sqrt{N}$  for  $0 \leq \phi \lesssim 0.9999$ , i.e.,  $\hat{\phi}$  can be much larger than  $\phi$  facilitating, thereby, the attainment of EMI with subplanckian  $\phi$ 's. This output is welcome, since SUGRA can be traditionally viewed as an effective theory valid for superfield values below  $m_P$ .

### 3.2 Inflationary potential

The only surviving term in Eq. (20c) along the trough in Eq. (21) is

$$V_E = \langle V_F \rangle_I = \langle e^K K^{SS^*} |W_{,S}|^2 \rangle_I, \tag{29}$$

where Eqs. (5a), (5b) yield

$$\langle e^K \rangle_I = \begin{cases} f_p^{-N} & \text{for } K = K_{12}, \\ 1 & \text{for } K = \tilde{K}_{12}, \end{cases} \tag{30}$$

i.e., the pole in  $f_p$  is presumably present in  $V_E$  of  $\delta\text{EM}$ , but it disappears in  $V_E$  of  $\text{EM2}$  and  $\text{EM4}$ , as anticipated by the model's description in Sect. 1. Substituting Eqs. (3) and (30) into Eq. (29), this takes its master form

$$V_E = \begin{cases} (\lambda_1\phi + \lambda_2\phi^2 - M^2)^2 / f_p^N & \text{for } \delta\text{EM}, \\ (\lambda_1\phi + \lambda_2\phi^2 - M^2)^2 & \text{for EM2 and EM4.} \end{cases} \tag{31}$$

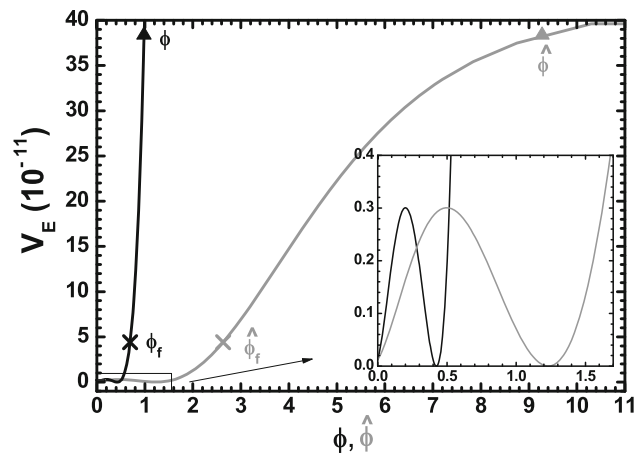


**Fig. 1** Inflationary potential  $V_E$  for EM4 as a function of  $\phi$  (black line) for  $\phi > 0$  and  $\hat{\phi}$  (gray line) for  $\hat{\phi} > 0$ . We set  $r_{12} = 0.4$ ,  $M_2 = 0.1$  and  $N = 10$ . Values corresponding to  $\phi_*$  [ $\hat{\phi}$ ] and  $\phi_f$  [ $\hat{\phi}_f$ ] are depicted. Shown is also the low- $\phi$  behavior of  $V_E$  in the inset

The formula above can be brought in the more compact form

$$V_E = \lambda^2 \begin{cases} (\phi - r_{21}\phi^2 - M_1^2)^2 / f_p^N & \text{for } \delta\text{EM}, \\ (\phi - r_{21}\phi^2 - M_1^2)^2 & \text{for EM2}, \\ (\phi^2 - r_{12}\phi - M_2^2)^2 & \text{for EM4,} \end{cases} \tag{32}$$

if we defined the ratios  $r_{ij} = -\lambda_i/\lambda_j$  with  $i, j = 1, 2$  and identify  $\lambda$  and  $M_i$  as follows

$$\lambda = \begin{cases} \lambda_1 \text{ and } M_1 = M/\sqrt{\lambda_1} & \text{for } \delta\text{EM and EM2,} \\ \lambda_2 \text{ and } M_2 = M/\sqrt{\lambda_2} & \text{for EM4.} \end{cases} \tag{33}$$

From the first relation in Eq. (32), we easily infer that the elimination of the pole from the denominator of  $V_E$  can be implemented if we set  $N = 2$  and take  $\delta_{21} = r_{21} - 1$  and  $M_1$  to tend to zero. On the other hand, no  $N$  dependence in  $V_E$  arises for  $\text{EM2}$  and  $\text{EM4}$ .

The activation of the inflationary stage in our models is pretty stable and well known [4,5,10]. It is based on the fact that  $V_E$  expressed in terms of  $\hat{\phi}$  develops a plateau for  $\hat{\phi} \gg 1$  but  $\phi < 1$  – since  $\hat{\phi}$  increases w.r.t  $\phi$  as inferred from Eq. (28). This key feature is clearly demonstrated in Fig. 1 where we comparatively plot  $V_E$  for  $\text{EM4}$  as a function of  $\phi$  (black line) and  $\hat{\phi}$  (gray line) – similar behavior is expected for  $\delta\text{EM}$  and  $\text{EM2}$ . We use  $N = 10$ ,  $M_2 = 0.1$  and  $r_{12} = 0.4$  resulting, via the inflationary constraints – see Sect. 4.1 –, to  $\lambda_2 = 3.5 \cdot 10^{-5}$ . We see that  $V_E$  experiences a stretching for  $\hat{\phi} > 1$  which results to a plateau facilitating, thereby, the establishment of EMI. The two crucial values of  $\phi$  [ $\hat{\phi}$ ]  $\phi_f = 0.69$  [ $\hat{\phi}_f = 2.63$ ] and  $\phi_* = 0.984$  [ $\hat{\phi}_* = 9.27$ ] which are defined in Sect. 4.1 and limit the observationally relevant inflationary period are also depicted.

### 3.3 SUSY vacuum and inflaton mass

Another important issue related to  $V_E$  is the structure of the SUSY vacuum. For  $\delta EM$  and EM2 the extremization condition yields the following critical points

$$\phi_{1\pm} = \frac{1 \pm \sqrt{1 - 4r_{21}M_1^2}}{2r_{21}} \text{ and } \phi_{1c} = \frac{1}{2r_{21}}, \tag{34}$$

from which we easily conclude that the SUSY vacuum lies at  $\langle \phi \rangle = \phi_{1-}$ . Note that, for  $|r_{21}| \leq 1$ , we obtain  $\phi_{1+} > 1$  and so it is irrelevant for our scenario. To place the location of the maximum  $\phi_{1\max} = \phi_{1c}$  at the same invisible domain of  $\phi$  values, we impose

$$r_{21} \leq 1/2. \tag{35}$$

As a consequence, EMI can take place undoubtedly for  $\phi$  values in the range  $\langle \phi \rangle \leq \phi \leq 1$ . On the other hand, the constraint  $\langle \phi \rangle \leq 1$  yields a maximal  $M_1$  value which is

$$M_{1\max} = \begin{cases} \sqrt{1 - r_{21}}, & \text{if } r_{21} < 1/2, \\ 1/2r_{21} & \text{if } r_{21} \geq 1/2. \end{cases} \tag{36}$$

For  $\delta EM$ ,  $r_{21} \simeq 1$  and so only the latter bound is applicable. It is, though, overshadowed by the inflationary requirements which dictate  $M_1 \lesssim 0.01$  – see Sect. 4. For EM2, the bound of Eq. (35) cancels the second branch in Eq. (36).

A richer vacuum configuration arises for EM4. Indeed, the extrema of  $V_E$  turn out to be

$$\phi_{2\pm} = \frac{1}{2} \left( r_{12} \pm \sqrt{r_{12}^2 + 4M_2^2} \right) \text{ and } \phi_{2c} = \frac{r_{12}}{2}, \tag{37}$$

from which the former are minima whereas the latter is maximum. All of these are located below the pole position at  $\phi = 1$  for the relevant  $r_{12}$  values. Therefore, the SUSY vacuum lies at one of the two asymmetric  $\langle \phi \rangle = \phi_{2\pm}$ . The emergent situation is depicted in the inset of Fig. 1 where we obtain  $\langle \phi \rangle = 0.42$  or  $-0.023$  and  $\phi_{\max} = 0.2$ . The constraint  $\langle \phi \rangle \leq 1$  yields

$$M_2 \leq M_{2\max} = \sqrt{1 - r_{12}}. \tag{38}$$

The restrictions in Eqs. (36) and (38) for EM2 and EM4 are depicted in Fig. 2 where we plot the allowed values in the  $r_{21} - M_1$  plane EM2 and in  $r_{12} - M_2$  plane for EM4. We confine ourselves to the realistic ranges  $|r_{21}| \leq 1$  and  $|r_{12}| \leq 1$  where inflationary solution are detected.

The determination of  $\langle \phi \rangle$  from Eqs. (36) and (38) influences heavily the mass of the (canonically normalized) inflaton,

$$\widehat{\delta\phi} = \langle J \rangle \delta\phi \text{ with } \langle J \rangle = \sqrt{\frac{N}{2}} \langle f_p \rangle^{-1} \text{ \& } \delta\phi = \phi - \langle \phi \rangle \tag{39a}$$

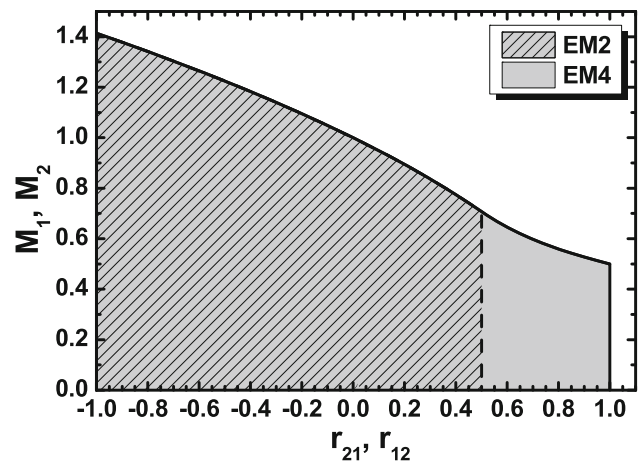


**Fig. 2** Allowed regions in the  $r_{21} - M_1$  (lined region) for EM2 and  $|r_{21}| \leq 1$  and in the  $r_{12} - M_2$  (gray region) plane for EM4 and  $|r_{12}| \leq 1$

which is given by

$$\widehat{m}_{\delta\phi} = \langle V_{E,\widehat{\phi\phi}} \rangle^{1/2} \simeq \begin{cases} 2\lambda_1/\sqrt{N} & \text{for } \delta EM \text{ \& } EM2, \\ 2r_{12}\lambda_2/\sqrt{N} & \text{or} \\ \frac{2r_{12}}{\sqrt{N}}(1 - r_{12})\lambda_2 & \text{for } EM4, \end{cases} \tag{39b}$$

where the last (approximate) equality is valid only for  $M \ll 1$ . Recall that we use  $N = 2$  for  $\delta EM$  and we obtain two possible vacua for EM4, as mentioned below Eq. (37). For the parameters employed in Fig. 1, we obtain  $\widehat{m}_{\delta\phi} = 10^{-5} m_P$  or  $5.6 \cdot 10^{-6} m_P$  corresponding to  $\langle \phi \rangle = \phi_+$  and  $\phi_-$  respectively. The precise value of  $\langle \phi \rangle$  requires a numerical study of the inflaton dynamics after EMI which is obviously beyond the scope of the present paper.

### 3.4 Radiative corrections

To consolidate our proposal we verify that the configuration in Eq. (21) is stable w.r.t the excitations of the non-inflaton fields. Taking into the limit  $\delta_{21} = M_1 = 0$  for  $\delta EM$ ,  $r_{21} = M_1 = 0$  for EM2 and  $r_{12} = M_2 = 0$  for EM4, we find the expressions of the masses squared  $\widehat{m}_{\chi^\alpha}^2$  (with  $\chi^\alpha = \theta$  and  $s$ ) arranged in Table 1. We there display the masses  $\widehat{m}_{\psi_\pm}^2$  of the corresponding fermions too – we define  $\widehat{\psi}_\Phi = J\psi_\Phi$  where  $\psi_\Phi$  and  $\psi_S$  are the Weyl spinors associated with  $S$  and  $\Phi$  respectively. We notice that the relevant expressions can take a unified form for all models – recall that we use  $N = 2$  in  $\delta EM$  – and approach, close to  $\phi = \phi_* \simeq 1$ , rather well the quite lengthy, exact ones employed in our numerical computation. From them we can appreciate the role of  $N_S < 6$  in retaining positive  $\widehat{m}_s^2$ . Also, we confirm that  $\widehat{m}_{\chi^\alpha}^2 \gg H_E^2 \simeq V_{E0}/3$  for  $\phi_f \leq \phi \leq \phi_*$ .

**Table 1** Mass spectrum along the path in Eq. (21) for EMI – we take  $n = 1$  for  $\delta$ EM and EM2 whereas  $n = 2$  for EM4

Fields	Eigestates	Mass squared	
1 real scalar	$\widehat{\theta}$	$\widehat{m}_\theta^2$	$6H_E^2$
2 real scalars	$\widehat{s}, \widehat{\bar{s}}$	$\widehat{m}_s^2$	$6H_E^2/N_S$
2 Weyl spinors	$(\psi_S \pm \widehat{\psi}_\Phi)/\sqrt{2}$	$\widehat{m}_{\psi_\pm}^2$	$6nf_p^2 H_E^2/N\phi^2$

Inserting the derived mass spectrum in the well-known Coleman-Weinberg formula, we can find the one-loop radiative corrections,  $\Delta V_E$  to  $V_E$ . Our inflationary results are immune from  $\Delta V_E$ , provided that the renormalization group mass scale  $Q$ , is determined by requiring  $\Delta V_E(\phi_\star) = 0$  or  $\Delta V_E(\phi_f) = 0$  – see the relevant detailed discussion in Ref. [30]. These conditions yield  $Q \simeq (0.25 - 9) \cdot 10^{-5}$  and eliminate any possible dependence of our results on the choice of  $Q$ . Under these circumstances, our results in the SUGRA set-up can be exclusively reproduced by using  $V_E$  in Eq. (32).

### 4 Inflation analysis

We here remind the basics of the inflation analysis in Sect. 4.1 and analyze the response of the proposed models analytically and numerically in Sects. 4.2 and 4.3 respectively.

#### 4.1 Preliminaries

Let us recall that the investigation of slow-roll EMI requires the computation of:

(a) The slow-roll parameters

$$\epsilon = \left( V_{E,\widehat{\phi}}/\sqrt{2}V_E \right)^2 \quad \text{and} \quad \eta = V_{E,\widehat{\phi\phi}}/V_E, \quad (40a)$$

which control the duration of EMI upon the condition

$$\max\{\epsilon(\phi), |\eta(\phi)|\} \leq 1. \quad (40b)$$

Its saturation at  $\phi = \phi_f$  or  $\widehat{\phi} = \widehat{\phi}_f$  signals the termination of EMI.

(b) The number of e-foldings  $N_\star$  that the scale  $k_\star = 0.05/\text{Mpc}$  experiences during EMI and the amplitude  $A_s$  of the power spectrum of the curvature perturbations generated by  $\phi$ . These observables can be calculated using the standard formulae

$$N_\star = \int_{\widehat{\phi}_f}^{\widehat{\phi}_\star} d\widehat{\phi} \frac{V_E}{V_{E,\widehat{\phi}}} \quad \text{and} \quad A_s = \frac{1}{12\pi^2} \frac{V_E^3}{V_{E,\widehat{\phi}}^2} \Bigg|_{\widehat{\phi}=\widehat{\phi}_\star}, \quad (41)$$

where  $\phi_\star$  [ $\widehat{\phi}_\star$ ] is the value of  $\phi$  [ $\widehat{\phi}$ ] when  $k_\star$  crosses the inflationary horizon.

(c) The (scalar) spectral index,  $n_s$ , its running,  $a_s$ , and the tensor-to-scalar ratio,  $r$ , found from the relations

$$n_s = 1 - 6\epsilon_\star + 2\eta_\star, \quad r = 16\epsilon_\star, \quad (42a)$$

$$a_s = 2 \left( 4\eta_\star^2 - (n_s - 1)^2 \right) / 3 - 2\xi_\star, \quad (42b)$$

where the variables with subscript  $\star$  are evaluated at  $\phi = \phi_\star$  and  $\xi = V_{E,\widehat{\phi}} V_{E,\widehat{\phi\phi\phi}} / V_E^2$ .

#### 4.2 Analytic results

Applying the formulas of the section above we here present an analytic approach to the dynamics of our models. Despite the fact that the formulae is presented in terms of the field  $\widehat{\phi}$ , we use as independent variable  $\phi$  taking advantage of Eqs. (32) and (27) and avoiding the direct reference to  $V_E = V_E(\widehat{\phi})$  which is more complicated. In particular, Sects. 4.2.1, 4.2.2 and 4.2.3 are devoted to  $\delta$ EM, EM2 and EM4 respectively.

##### 4.2.1 $\delta E$ model ( $\delta$ EM)

For the present model we set  $N = 2$  – see Sect. 3.2. The slow-roll parameters read

$$\epsilon \simeq \frac{2f_p^2}{\phi^2} - \frac{4}{\phi^3} \left( \delta_{21}\phi^2 - 2M_1^2(1 - 2\phi) \right); \quad (43a)$$

$$\eta \simeq 2 \left( 2 + \frac{1}{\phi^2} - \frac{3}{\phi} \right) + \frac{2}{f_p\phi^3} \left( \delta_{21}\phi^2(3\phi - 4) + M_1^2(2 + \phi(4\phi - 7)) \right). \quad (43b)$$

The condition of Eq. (40b) in the present case implies

$$\phi_f \simeq \max \left\{ 2 - \sqrt{2}, \sqrt{3} - 1 \right\}, \quad (44)$$

i.e.,  $\phi_f$  is determined due to the violation of the  $\eta$  criterion. Assuming  $\phi_f \ll \phi_\star$ ,  $N_\star$  can be approximately computed from Eq. (41) as follows

$$N_\star \simeq \frac{1}{2} \frac{\phi_\star}{1 - \phi_\star} \Rightarrow \phi_\star \simeq \frac{2N_\star}{2N_\star + 1}, \quad (45)$$

where any dependence on the parameters  $\delta_{21}$  and  $M$  can be safely ignored. From the last expression, we infer that  $\phi_\star$  is slightly lower than unity. Plugging  $\phi_\star$  from Eq. (45) into the rightmost equation in Eq. (41) and solving w.r.t  $\lambda$ , we arrive at the expression

$$\lambda = 2\sqrt{3}A_s\pi/N_\star, \quad (46)$$

which yields values comparable to the ones obtained for the quartic power-law model [18]. Upon substitution of  $\phi_\star$  into Eqs. (42a) and (42b), we obtain the observational predictions of  $\delta EM$  which are

$$n_s \simeq 1 - \frac{2}{N_\star} \left( 1 + \delta_{21} + \frac{M_1^2}{2} \right) + 4(\delta_{21} + M_1^2)(1 - 4N_\star); \tag{47a}$$

$$r \simeq \frac{8}{N_\star^2} \left( \frac{1 - 4(\delta_{21} + M_1^2)N_\star^2}{1 - 2(\delta_{21} + M_1^2)N_\star} \right)^2 \quad \text{and} \quad a_s \sim -\frac{3}{N_\star^2}, \tag{47b}$$

where the last expression (for  $a_s$ ) yields just an order of magnitude estimation. From Eq. (47a) we expect that small deviations of  $\delta_{21}$  from zero are capable to generate sizable deviations of  $n_s$  from its value within original Starobinsky inflation. Such a deviation is not possible for  $r$ .

#### 4.2.2 E model 2 (EM2)

The slow-roll parameters are here estimated as follows

$$\epsilon \simeq \frac{4f_p^2}{N} \left( \frac{1 - 2r_{21}\phi}{\phi(1 - r_{21}\phi) - M^2} \right)^2; \tag{48a}$$

$$\eta \simeq \frac{4f_p}{N} \frac{1 - (2 + 3r_{21}(2 - 3\phi))\phi}{(\phi(1 - r_{21}\phi) - M^2)^2}, \tag{48b}$$

with the  $N$  dependence being explicitly displayed. The condition of Eq. (40b) yields

$$\phi_f \simeq \max \left\{ 2 \frac{2 - \sqrt{N}}{4 - \sqrt{N}}, 2 \frac{3 - \sqrt{1 - N}}{8 - N} \right\}. \tag{49}$$

For  $N \sim \mathcal{O}(10)$ ,  $\phi_f$  turns out to be close to  $\phi_\star \sim 1$ . Therefore, an accurate analytic estimation of  $N_\star$  may include both contributions as follows

$$N_\star = I_N(\phi_\star) - I_N(\phi_f), \tag{50}$$

where the function  $I_N$ , found performing the integration in Eq. (41), takes the form

$$I_N(\phi) = (N/8f_{21}^2) \left( 2f_{21}(1 - r_{21} - M_1^2)/f_p + 2(f_{21} + 2r_{21}^2) \ln f_p - \ln(1 - 2r_{21}\phi) \right), \tag{51}$$

with  $f_{21} = 1 - 2r_{21}$ . I.e., as  $r_{21}$  approaches its maximum,  $1/2$ , in Eq. (35)  $I_N(\phi)$  gets enhanced causing via Eq. (50) a sizeable deviation of  $N_\star$  from its result obtained for a monomial  $V_E$ . In such a delicate situation, all three terms in the right-hand side of Eq. (51) are equally important and the analytic solution of  $N_\star$  w.r.t  $\phi$  is not doable. In this domain,

the numerical computation is our last resort. Focusing on  $r_{21} \ll 0.5$ , neglecting  $I_N(\phi_f)$  and the logarithmic contributions from  $I_N(\phi_\star)$  in Eq. (50), we may solve Eq. (50) w.r.t  $\phi_\star$  with result

$$\phi_\star \simeq 4f_{21}N_\star / (4N_\star f_{21} + N(1 - r_{21} - M_1^2)). \tag{52}$$

Comparing with the numerical results we verify that the estimation above is more and more accurate as  $N, r_{21}$  and  $M_1$  decrease below 10, 0.5 and 0.1 respectively. Plugging  $\phi_\star$  from Eq. (52) into the rightmost equation in Eq. (41) and solving w.r.t  $\lambda$  we find

$$\lambda \simeq \sqrt{3NA_s/2(4N_\star + N)}\pi/2N_\star^2. \tag{53}$$

Inserting Eq. (52) into Eqs. (42a) and (42b) and performing an expansion in series for low  $1/N_\star$  we obtain

$$n_s \simeq 1 - \frac{2}{N_\star} - \frac{N}{N_\star^2 f_{21}^2} \left( 1 - \frac{5}{2}r_{21} - 3r_{21}^2 - \frac{1}{2}M_1^2 \right); \tag{54a}$$

$$r \simeq \frac{4N}{N_\star^2 f_{21}^2} \left( 1 - \left( 8 - N(1 + 4M_1^2) \right) r_{21}/2 + 4r_{21}^2 + NM_1^2/2 \right); \tag{54b}$$

$$a_s \simeq \frac{2}{N_\star^2} - \frac{N}{N_\star^3 f_{21}^2} \left( \frac{5}{2} + (6 + 7M_1^2)r_{21} - 7r_{21}^2 - M_1^2 \right). \tag{54c}$$

For  $f_{21} \simeq 1$  (i.e.  $r_{21} \simeq 0$ ) the results above reduce to the well-known predictions of  $\alpha$ -attractors – recall that our results can be directly compared with those in Refs. [10, 19] setting  $N = 3\alpha$ .

#### 4.2.3 E model 4 (EM4)

Repeating the steps followed in the previous sections, we can obtain the corresponding formulas for EM4. In particular, the slow-roll parameters read

$$\epsilon \simeq \frac{4f_p^2}{N} \left( \frac{2\phi - r_{12}}{\phi^2 - r_{12}\phi - M_2^2} \right)^2; \tag{55a}$$

$$\eta \simeq \left( 4f_p/N(\phi^4 - r_{12}\phi - M_2^2)^2 \right) \left( 2\phi^2(3 - 4\phi) - 2M_2^2(1 - 2\phi) + r_{12}^2(1 - 2\phi) + 3r_{12}(3\phi - 2\phi) \right). \tag{55b}$$

The condition of Eq. (40b) implies

$$\phi_f \simeq \max \left\{ 4 \frac{4 - \sqrt{N}}{16 - \sqrt{N}}, 2 \frac{14 - \sqrt{2}\sqrt{2 + 3N}}{32 - N} \right\}. \tag{56}$$

As in Sect. 4.2.2, the reliable estimation of  $N_*$  requires the application of Eq. (50) where the function  $I_N$  is now given by

$$I_N(\phi) = (N/8f_{12}^2) \left( 2f_{12}(1 - r_{12} - M_2^2)/f_p + 2(f_{12} - r_{12} + r_{12}^2) \ln f_p - r_{12}^2 \ln(2\phi - r_{12}) \right) \tag{57}$$

with  $f_{12} = 2 - r_{12}$ . Note that Eq. (38) protects the present case from the appearance of any pole in the equation above. We may then solve Eq. (50) w.r.t  $\phi_*$  with result

$$\phi_* \simeq 4f_{12}N_*/(4f_{12}N_* + (1 - r_{12} - M_2^2)N), \tag{58}$$

where we neglected  $I_N(\phi_f)$  and the logarithmic contributions from  $I_N(\phi_*)$ . Plugging the expression above into the rightmost equation in Eq. (41) we find

$$\lambda \simeq \sqrt{3N A_s/2(8N_* + N)^2\pi/32N_*^3}. \tag{59}$$

Moreover, substitution of Eq. (58) into Eqs. (42a) and (42b) yields

$$n_s \simeq 1 - \frac{2}{N_*} - \frac{N}{N_*^2 f_{21}^2} \left( 3 - \frac{5}{2}r_{12} - r_{12}^2 + 3M_2^2 \right); \tag{60a}$$

$$r \simeq \frac{16N}{N_*^2 f_{12}^2} \left( 1 - (1 - N/8N_* - r_{12}/4)r_{12} + NM_2^2(4 - r_{12}/N)/8N_* \right); \tag{60b}$$

$$a_s \simeq -\frac{8}{N_*^3 f_{21}^2} \left( 1 - r_{12} + r_{12}^2/4 + 7N/8N_* \right). \tag{60c}$$

Again, for  $f_{12} \simeq 2$  (i.e.  $r_{12} \simeq 0$ ) the results above reduce to the well-known predictions of  $\alpha$ -attractors [10, 19].

### 4.3 Numerical results

Our analytic findings above can be checked and extended for any value of the relevant parameters numerically. At first, we confront the quantities in Eq. (41) with the observational requirements [31]

$$N_* \simeq 61.3 + \frac{1 - 3w_{\text{rh}}}{12(1 + w_{\text{rh}})} \ln \frac{\pi^2 g_{\text{rh}*} T_{\text{rh}}^4}{30V_E(\phi_f)} + \frac{1}{4} \ln \frac{V_E(\phi_*)^2}{g_{\text{rh}*}^{1/3} V_E(\phi_f)} \text{ and } A_s \simeq 2.105 \cdot 10^{-9}, \tag{61}$$

where we assume that EMI is followed in turn by an oscillatory phase with mean equation-of-state parameter  $w_{\text{rh}}$ , radiation and matter domination. Motivated by implementations [35–37] of non-thermal leptogenesis, which may follow EMI, we set  $T_{\text{rh}} \simeq 10^9$  GeV for the reheat temperature. Also, we

take for the energy-density effective number of degrees of freedom  $g_{\text{rh}*} = 228.75$  which corresponds to the MSSM spectrum. Note that this  $T_{\text{rh}}$  avoids exhaustive tuning on the relevant coupling constant involved in the decay width of the inflaton – cf. Ref. [16].

Due to the polynomial character of  $V_E$  in Eq. (32) and the non-minimal kinetic mixing in Eq. (27), the estimation of  $w_{\text{rh}}$  requires some care – cf. Refs. [33, 34]. We determine it adapting the general formula [32], i.e.

$$w_{\text{rh}} = 2 \frac{\int_{\phi_{\text{mn}}}^{\phi_{\text{mx}}} d\phi J(1 - V_E/V_E(\phi_{\text{mx}}))^{1/2}}{\int_{\phi_{\text{mn}}}^{\phi_{\text{mx}}} d\phi J(1 - V_E/V_E(\phi_{\text{mx}}))^{-1/2}} - 1, \tag{62}$$

where  $\phi_{\text{mn}} = \langle \phi \rangle$  is given by Eq. (34) for  $\delta\text{EM}$  and  $\text{EM2}$  or Eq. (37) for  $\text{EM4}$ – in the latter case we assume that  $\langle \phi \rangle = \phi_+$  which is considered as more probable than the  $\langle \phi \rangle = \phi_-$ . The amplitude of the oscillations during reheating  $\phi_{\text{mx}}$  is found by solving numerically the condition  $\sqrt{3}H_E(\phi_{\text{mx}}) = \hat{m}_1$  if  $\sqrt{3}H_E(\phi_f) > \hat{m}_1$  or it is  $\phi_{\text{mx}} = \phi_f$  otherwise. Performing an expansion for low  $\phi_{\text{mx}}$  values we can obtain the following approximate expression

$$w_{\text{rh}} \simeq -\frac{2\phi_{\text{mx}}}{3\pi} + \left( \frac{4}{3\pi^2} - \frac{1}{4} \right) \phi_{\text{mx}}^2 + \frac{\pi^2 - 80}{30\pi^3} \phi_{\text{mx}}^3 \tag{63a}$$

for  $\delta\text{EM}$  where  $r_{21} \simeq 1$ . For  $\text{EM2}$ , where  $r_{21} \neq 1$  the corresponding expression takes the form

$$w_{\text{rh}} \simeq -\frac{2\phi_{\text{mx}}}{3\pi}(1 + 2r_{21}) + \phi_{\text{mx}}^2 \left( \frac{4}{3\pi^2} + \frac{16r_{21}}{3\pi^2} + \frac{2r_{21}}{3\pi} - \frac{1}{4}(1 + 3r_{21}) \right). \tag{63b}$$

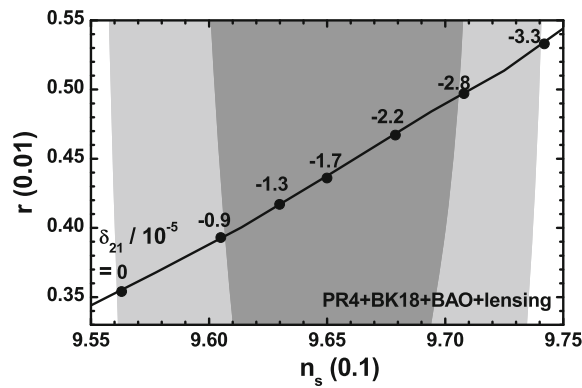
It was not doable to obtain similar formula for  $\text{EM4}$ , for which we trust our numerical result. These refinements result to a reduction of  $w_{\text{rh}}$  w.r.t its value for a pure quadratic ( $w_{\text{rh}} = 0$ ) or quartic ( $w_{\text{rh}} = 1/3$ ) potential.

Enforcing Eq. (61) we can restrict  $\lambda$  and  $\phi_*$  via Eq. (41). In general, we obtain  $\lambda \simeq (0.1 - 5.4) \cdot 10^{-5}$  in agreement with Eqs. (46),(53) and (59). Regarding  $\phi_*$  we assume that  $\phi$  starts its slow roll below the location of kinetic pole, i.e.,  $\phi = 1$ , consistently with our approach to SUGRA as an effective theory below  $m_P = 1$ . The closer to pole  $\phi_*$  is set the larger  $N_*$  is obtained. Therefore, a tuning of the initial conditions is required which can be somehow quantified defining the quantity

$$\Delta_* = (1 - \phi_*). \tag{64}$$

The naturalness of the attainment of EMI increases with  $\Delta_*$ . After the extraction of  $\lambda$  and  $\phi_*$ , we compute the models' predictions via Eqs. (42a) and (42b), for any selected values for the remaining parameters. Our outputs are encoded as





$(n_s/0.1, r/0.01)$	$M_1 = 0.001$	$M_1 = 0.005$	$M_1 = 0.01$
	$-\delta_{21}/10^{-5}$	$-\delta_{21}/10^{-5}$	$-\delta_{21}/10^{-4}$
(9.56, 0.35)	0	2.45	0.98
(9.61, 0.39)	0.9	3.25	1.08
(9.65, 0.44)	1.7	4.1	1.15
(9.71, 0.5)	2.8	5.2	1.26
(9.74, 0.53)	3.3	5.7	1.315

**Fig. 3** Allowed curve in the  $n_s - r$  plane for  $\delta$ EM with  $M_1 = 0.001$  and various  $\delta_{21}$ 's indicated on the line. The marginalized joint 68% [95%] c.l. regions [40] from PR4, BK18, BAO and lensing data-sets [39] are depicted by the dark [light] shaded contours. The allowed curve remains essentially unaltered if we set  $M_1 = 0.005$  or  $0.01$ . The variation some of the  $\delta_{21}$  values indicated in the plot is shown in the table

lines in the  $n_s - r$  plane and compared against the observational data [39] in Figs. 3 for  $\delta$ EM and 4 for EM2 and EM4. We take into account the latest *Planck release 4* (PR4) – including TT,TE,EE+lowlEB power spectra [38] –, *Baryon Acoustic Oscillations* (BAO), CMB-lensing and BICEP/Keck (BK18) data [39]. Fitting it [40] with  $\Lambda$ CDM we obtain the marginalized joint 68% [95%] regions depicted by the dark [light] shaded contours in the aforementioned figures. Approximately we obtain

$$n_s = 0.965 \pm 0.009 \text{ and } r \lesssim 0.032, \tag{65}$$

at 95% confidence level (c.l.) with negligible  $a_s$ . The results are exposed separately in Sect. 4.3.1 for  $\delta$ EM and 4.3.2 for EM2 and EM4.

Let us note here, that urged by similar investigations [16], we performed a numerical comparison of our results with those obtained if we use the second-order slow-roll formulation [41,42]. We verified that  $\widehat{N}_* - N_* \simeq 1 - 2$  where  $\widehat{N}_*$  is the corrected  $N_*$  value. This refinement, though, has negligible impact on  $n_s$ ,  $a_s$  and  $r$  and so it does not affect our results to any essential way.

### 4.3.1 $\delta$ E Model ( $\delta$ EM)

Let, initially, recall that the remaining free parameters of  $\delta$ EM are just two,  $\delta_{21}$  and  $M_1$ . As explained in Sect. 3.2, the

cancellation of  $f_p$  from the denominator of  $V_E$  in Eq. (32) requires a synergy between the conditions  $N = 2$ ,  $M_1 \ll 1$  and a tuning on  $r_{21}$  – cf. Refs. [4,5,8,9,15]. This unavoidable tuning is qualified through the parameter  $\delta_{21} = r_{21} - 1$  which is varied along the curve of Fig. 3 fixing  $M_1 = 0.001$ . We notice that  $\delta_{21}$  is stuck at the level  $10^{-5}$ . Practically this result is intact for any lower  $M_1$  value. Varying  $M_1$  for  $0 \leq M_1 \leq 0.02$  we can obtain a line undistinguished from that shown in Fig. 3 with the depicted points  $(n_s, r)$  corresponding to readjusted  $\delta_{21}$  values, though. For some sample  $M_1$  values,  $M_1 = 0.005$  and  $0.01$ , the outputs of this readjustment are listed in the Table in Fig. 3. We see that increasing  $M_1$  the tuning on  $\delta_{21}$  is slightly ameliorated. The increase of  $M_1$ , however, is severely limited from the viability of the EMI setting. The resulting  $n_s$  and  $r$  increase with  $M_1$  and  $\delta_{21}$ . This increase, though, is more drastic for  $n_s$  which covers the whole allowed range in Eq. (65). From the considered data we collect the results

$$-1.315 \cdot 10^2 \lesssim \delta_{21}/10^{-6} \lesssim 0, \quad 9 \cdot 10^{-3} \lesssim \Delta_* \lesssim 0.01, \tag{66a}$$

$$0.9 \lesssim -a_s/10^{-3} \lesssim 1.4 \text{ and } 3.6 \lesssim \widehat{m}_{\delta\phi}/10^{13}\text{GeV} \lesssim 5 \tag{66b}$$

with  $(n_s, r)$  varying in the range indicated in the Table of Fig. 3. Here and hereafter, we restore for convenience units regarding the results on  $\widehat{m}_{\delta\phi}$ . In all cases, we obtain  $N_* \simeq 44$  consistently with Eq. (61) and the resulting  $w_{\text{th}} \simeq -0.237$  from Eq. (63a). The achieved  $r$  values are of the order of  $10^{-3}$  and may be testable by the next-generation of polarized CMB space missions, like LiteBIRD [43].

### 4.3.2 E models 2 and 4

Turning now to EM2 and EM4, we remind that the remaining free parameters are  $N$ , and  $r_{21}$  and  $M_1$  for EM2 or  $r_{12}$  and  $M_2$  for EM4 – see Eq. (32). Our results for these models are presented in Fig. 4 and Table 2. In the figure above, we present the allowed curves in the  $n_s - r$  plane varying  $N$  along them and fixing the other parameters to some representative values.

Focusing first on the left plot of Fig. 4, devoted to EM2, we see that the solid, dashed, and dot-dashed lines are plotted for  $r_{21} = 0.001, 0.4$  and  $-0.4$  correspondingly and  $M_1 = 0.01$ . Along these lines  $N_* \simeq 50$  with  $w_{\text{th}} \simeq -(0.05 - 0.1)$  from Eq. (63b) independently from the parameters  $M_1$  and  $r_{21}$ . As a consequence [32],  $V_E$  for  $\phi$  close to  $\langle\phi\rangle$  behaves largely as a quadratic potential. We remark that the results for  $r_{21} = 0.001$  and  $-0.4$  yield  $n_s$  a little lower than its central value in Eq. (65). Interestingly enough, as  $r_{21}$  approaches its upper bound in Eq. (35) – and  $f_{21}$  in the denominator of the function  $I_N$  in Eq. (51) approaches zero –,  $n_s$  increases slightly and

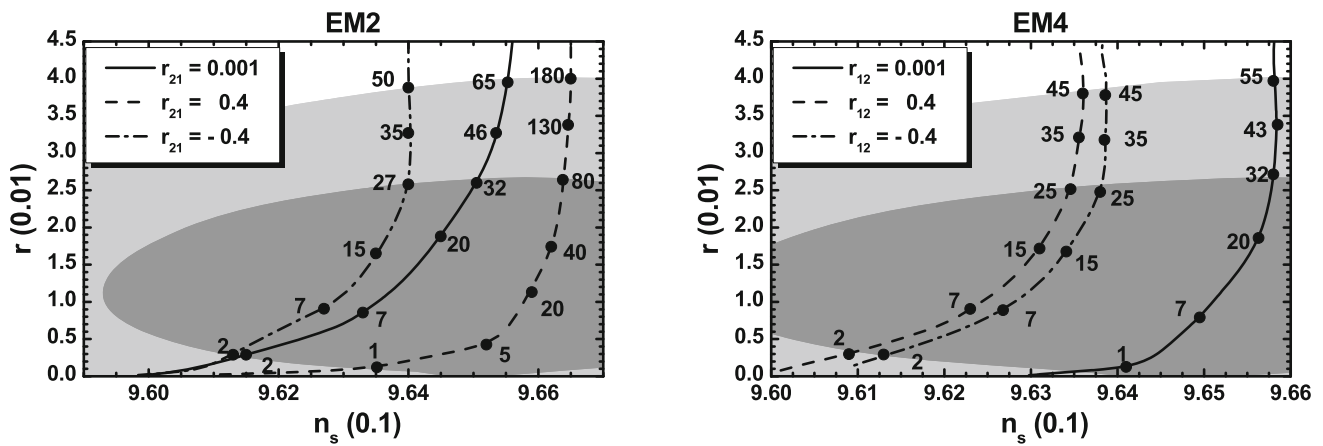


**Fig. 4** Allowed curves in the  $n_s - r$  plane for EM2,  $M_1 = 0.01$ , and  $r_{21} = 0.001$  (solid line),  $r_{21} = 0.4$  (dashed line),  $r_{21} = -0.4$  (dot-dashed line) or EM4,  $M_2 = 0.01$ , and  $r_{12} = 0.001$  (solid lines),

$r_{12} = 0.4$  (dashed line),  $r_{12} = -0.4$  (dot-dashed line). The points indicated on the curves correspond to various  $N$  values. The shaded corridors are identified as in Fig. 3

**Table 2** Parameters and observables for  $N = 10$ , EM2 and  $M_1 = 0.5$  or EM4 and  $M_2 = 0.5$

Model:	EM2 with $r_{21}$ values:			EM4 with $r_{12}$ values:		
	0.001	0.4	-0.4	0.001	0.4	-0.4
$\phi_*/0.1$	9.686	9.5	9.73	9.84	9.9	9.795
$\Delta_*(\%)$	3.1	5	2.7	1.6	0.9	2
$\phi_f/0.1$	5.4	5.3	5.4	7.1	8.4	6.2
$w_{th}$	-0.08	-0.11	-0.06	-0.04	-0.06	-0.029
$N_*$	49.2	49.7	50.5	50.3	49.8	50.5
$\lambda/10^{-5}$	2.7	4.7	1.7	2.7	5.8	1.8
$n_s/0.1$	9.62	9.65	9.62	9.62	9.63	9.62
$-a_s/10^{-4}$	7.4	6.8	7.2	7.2	7.1	7.2
$r/10^{-2}$	1.2	0.8	1.2	1.2	1.2	1.2

becomes precisely equal to its central value in Eq. (65) – see the dashed line corresponding to  $r_{21} = 0.4$  in the left plot of Fig. 4. In the same regime we also remark that the upper bound on  $N$  from Eq. (65) is sharply increased enhancing  $\Delta_*$  too. Unfortunately, the analytic formulas in Eqs. (54a), (54b) fail to explain further this observation since these are not valid in this regime. The variation of our results increasing  $M_1$  beyond 0.01, can be inferred by the three leftmost columns of Table 2, where we fix  $N = 10$  and  $M_1 = 0.5$  and list the outputs for the three  $r_{12}$  values used in the left plot of Fig. 4. We notice that our conclusions regarding the increase of  $n_s$  and  $\Delta_*$  as  $r_{21}$  approaches 0.5 insist. From the relevant data, we find the following allowed ranges of parameters

$$0.1 \leq N \leq 180, 0.961 \lesssim n_s \lesssim 0.966, 0.00015 \lesssim r \lesssim 0.4, \tag{67a}$$

$$0.014 \lesssim \Delta_*/0.1 \lesssim 3.4 \text{ and } 1.9 \lesssim \widehat{m}_{\delta\phi}/10^{13}\text{GeV} \lesssim 5.6, \tag{67b}$$

where we set an artificial lower bound on  $N$ , 0.1 to evade extensive (theoretical) tuning. The maximal  $\Delta_*$  and  $n_s$  values are encountered for  $r_{21} = 0.4$ , whereas  $a_s$  varies in the range  $-(6.6 - 7.7) \cdot 10^{-4}$ .

We proceed now with the investigation of EM4. Fixing  $M_2 = 0.01$  we present the allowed solid, dashed and dot-dashed curves in the right plot of Fig. 4 corresponding to  $r_{12} = 0.001, 0.4$  and  $-0.4$  respectively. In this case, the  $w_{th}$  values fluctuates widely – depending on  $r_{12}$  and  $M_2$  – which influences  $N_*$  via Eq. (61). Namely, for  $M_2 \lesssim 0.01$  and  $r_{12} \lesssim 0.1$  we obtain  $w_{th} \simeq (0.25 - 0.39)$  which results to  $N_* \simeq (54 - 56)$  whereas for larger  $M_2$  and  $r_{12}$  values we obtain  $w_{th} \simeq (0.0 - 0.086)$  which yields  $N_* \simeq (50 - 53)$ . I.e., in the former case,  $V_E$  for  $\phi \ll 1$  behaves as a quadratic potential whereas for the latter it approaches the quartic potential [32]. The augmentation of  $N_*$  for low  $r_{12}$  (and  $M_2$ ) values increases  $n_s$  which converges towards the “sweet” spot of the recent data in Eq. (65), as shown in the right plot of Fig. 4. Indeed, the solid line, corresponding to  $r_{12} = 0.001$  and  $M_2 = 0.01$ , for  $N \gtrsim 7$  passes from  $n_s$  values close to the central one in Eq. (65). The variation of our results increasing  $M_2$  beyond 0.01, can be inferred by the three rightmost columns of Table 2, where we fix  $N = 10$  and  $M_2 = 0.5$  and list the outputs for the three  $r_{12}$  values used in the right plot of Fig. 4. Since  $M_2$  is larger than 0.1 we obtain  $w_{th} \simeq -0.05$  – i.e. a quadratic-like potential –, and  $N_* \simeq 50$  and so  $n_s \simeq 0.963$ . Comparing with the data of the plot we conclude that increasing  $M_2$ , the required  $\phi_*$  slightly increases lowering the tuning. In total, for EM4 we

obtain

$$0.1 \leq N \leq 55, \quad 0.961 \lesssim n_s \lesssim 0.965, \quad 0.00013 \lesssim r \lesssim 0.4, \quad (68a)$$

$$0.1 \lesssim \Delta_*/0.01 \lesssim 8 \quad \text{and} \quad 1.2 \lesssim \widehat{m}_{\delta\phi}/10^{13}\text{GeV} \lesssim 2.2. \quad (68b)$$

The minimal values of  $n_s$  and  $r$  are 0.961 and 0.0007, respectively, encountered for the minimal  $N$  value considered, 0.1 whereas  $a_s \simeq -0.0007$  constantly. As regards  $\Delta_*$ , we see that tuning becomes milder w.r.t  $\delta\text{EM}$  but worse w.r.t that in EM2. In general it is a little improved compared to the models in Refs. [4,5].

From the results above, we clearly infer that the polynomial form of  $W$  in Eq. (3) has observational consequences which render our models explicitly distinguishable from the usually adopted monomial EMI [16–18].

## 5 Conclusions

Embarking on the fact that EMI (i.e., E-model inflation) is realized by the potential shown in Eq. (1), we introduced the Kähler potentials in Eqs. (5a) and (5b) which naturally yield the required  $\phi(\widehat{\phi})$  function in Eq. (2) connecting the initial,  $\phi$ , with the canonically normalized,  $\widehat{\phi}$ , inflaton. We then explored the hyperbolic geometry of the adopted  $K$ 's and showed that they are invariant under the set of transformations in Eq. (11a) composing a set of matrices  $\mathbf{M}$  in Eq. (13) which can be related to the group  $U(1, 1)$  – see Eq. (14). Despite the fact that their Kähler manifold does not enjoy a widely recognized symmetry, the proposed  $K$ 's can coexist with the superpotential  $W$  in Eq. (3) which is quite generic, renormalizable and consistent with an  $R$  symmetry. The emerging scalar potential gives rise to three inflationary models ( $\delta\text{EM}$ , EM2 and EM4) with potentials given in Eq. (32). Within  $\delta\text{EM}$  the denominator of the potential is cancelled out for  $N = 2$ , low  $M$  values and  $\lambda_2 \simeq -\lambda_1$  whereas the lack of denominator in EM2 and EM4 frees  $N$ ,  $\lambda_1$ ,  $\lambda_2$  and  $M$ .

All the models excellently match the observations by restricting the free parameters to reasonably ample regions of values. In particular, within  $\delta\text{EM}$  any observationally acceptable  $n_s$  is attainable by tuning  $\delta_{21}$  to values of the order  $10^{-5}$ , whereas  $r$  is kept at the level of  $10^{-3}$  – see Eq. (66a). On the other hand, EM2 and EM4 avoid any tuning, larger  $r$ 's are achievable as  $N$  increases beyond 2, while  $n_s$  lies close to its central value – see Eq. (67a). For both latter models, we localized portions of the allowed parameter space with  $n_s$  precisely equal to its central observational value. The inflaton mass is collectively confined to the range  $(1.2 - 5.6) \cdot 10^{13}$  GeV.

Comparing our setting with those [12–14] which employ the half-plane parameterization of the  $SU(1, 1)/U(1)$  Kähler manifold and display also a kinetic pole of order one placed at zero, we should note that the translation of the pole at unity within our framework, although trivial at a first sight, leads to the following far-reaching consequences: (i) it changes the geometry of the internal space; (ii) it allows  $W$  to assume a simple and generic form controlled by an  $R$  symmetry; (iii) it offers a more sizable variation of the observables due to the extra free parameters. For these reasons, we believe that the predictive, economical and observationally-friendly EMI can be comfortably implemented within the framework described in this paper.

**Acknowledgements** I would like to thank S. Ketov and E.W. Kolb for interesting discussions. This research work was supported by the Hellenic Foundation for Research and Innovation (H.F.R.I.) under the “First Call for H.F.R.I. Research Projects to support Faculty members and Researchers and the procurement of high-cost research equipment Grant” (Project Number: 2251).

**Data Availability Statement** This manuscript has no associated data or the data will not be deposited. [Authors' comment: We did not deposit data since the results shown in the paper are based on the formulas exposed in it and they can be reproduced by simple publicly available programs.]

**Open Access** This article is licensed under a Creative Commons Attribution 4.0 International License, which permits use, sharing, adaptation, distribution and reproduction in any medium or format, as long as you give appropriate credit to the original author(s) and the source, provide a link to the Creative Commons licence, and indicate if changes were made. The images or other third party material in this article are included in the article's Creative Commons licence, unless indicated otherwise in a credit line to the material. If material is not included in the article's Creative Commons licence and your intended use is not permitted by statutory regulation or exceeds the permitted use, you will need to obtain permission directly from the copyright holder. To view a copy of this licence, visit <http://creativecommons.org/licenses/by/4.0/>.  
Funded by SCOAP<sup>3</sup>.

## References

1. T. Terada, Generalized pole inflation: hilltop, natural, and chaotic inflationary attractors. *Phys. Lett. B* **760**, 674 (2016). [arXiv:1602.07867](https://arxiv.org/abs/1602.07867)
2. B.J. Broy, M. Galante, D. Roest, A. Westphal, Pole inflation, shift symmetry and universal corrections. *J. High Energy Phys.* **12**, 149 (2015). [arXiv:1507.02277](https://arxiv.org/abs/1507.02277)
3. T. Kobayashi, O. Seto, T.H. Tatsuishi, Toward pole inflation and attractors in supergravity: chiral matter field inflation. *Prog. Theor. Phys.* **2017**(12), 123B04 (2017). [arXiv:1703.09960](https://arxiv.org/abs/1703.09960)
4. C. Pallis, Pole-induced Higgs inflation with hyperbolic Kaehler geometries. *J. Cosmol. Astropart. Phys.* **05**, 043 (2021). [arXiv:2103.05534](https://arxiv.org/abs/2103.05534)
5. C. Pallis,  $SU(2, 1)/(SU(2) \times U(1))$  B-L Higgs Inflation. *J. Phys. Conf. Ser.* **2105**(12), 12 (2021). [arXiv:2109.06618](https://arxiv.org/abs/2109.06618)
6. S. Karamitsos, A. Strumia, Pole inflation from non-minimal coupling to gravity. [arXiv:2109.10367](https://arxiv.org/abs/2109.10367)

7. B. Afshar, N. Riazi, H. Moradpour, Pole inflation in dRGT theory. [arXiv:2110.02278](https://arxiv.org/abs/2110.02278)
8. J. Ellis, D.V. Nanopoulos, K.A. Olive, No-scale supergravity realization of the Starobinsky model of inflation. *Phys. Rev. Lett.* **111**, 111301 (2013) (Erratum-ibid. 111(12), 129902 (2013)). [arXiv:1305.1247](https://arxiv.org/abs/1305.1247)
9. J. Ellis, D. Nanopoulos, K. Olive, Starobinsky-like inflationary models as avatars of no-scale supergravity. *J. Cosmol. Astropart. Phys.* **10**, 009 (2013). [arXiv:1307.3537](https://arxiv.org/abs/1307.3537)
10. R. Kallosh, A. Linde, D. Roest, Superconformal inflationary  $a$ -attractors. *J. High Energy Phys.* **11**, 198 (2013). [arXiv:1311.0472](https://arxiv.org/abs/1311.0472)
11. J. Ellis, D.V. Nanopoulos, K.A. Olive, S. Verner, A general classification of Starobinsky-like inflationary avatars of  $SU(2, 1)/SU(2) \times U(1)$  no-scale supergravity. *J. High Energy Phys.* **03**, 099 (2019). [arXiv:1812.02192](https://arxiv.org/abs/1812.02192)
12. J.J.M. Carrasco, R. Kallosh, A. Linde, D. Roest, Hyperbolic geometry of cosmological attractors. *Phys. Rev. D* **92**(4), 041301 (2015). [arXiv:1504.05557](https://arxiv.org/abs/1504.05557)
13. J.J.M. Carrasco, R. Kallosh, A. Linde,  $\alpha$ -Attractors: Planck, LHC and Dark Energy. *J. High Energy Phys.* **10**, 147 (2015). [arXiv:1506.01708](https://arxiv.org/abs/1506.01708)
14. J.J.M. Carrasco, R. Kallosh, A. Linde, Cosmological attractors and initial conditions for inflation. *Phys. Rev. D* **92**(6), 063519 (2015). [arXiv:1506.00936](https://arxiv.org/abs/1506.00936)
15. J. Ellis, M.A.G. Garcia, N. Nagata, D.V. Nanopoulos, K.A. Olive, S. Verner, Building models of inflation in no-scale supergravity. *Int. J. Mod. Phys. D* **29**(16), 2030011 (2020). [arXiv:2009.01709](https://arxiv.org/abs/2009.01709)
16. J. Ellis, M.A.G. Garcia, D.V. Nanopoulos, K.A. Olive, S. Verner, BICEP/Keck constraints on attractor models of inflation and reheating. *Phys. Rev. D* **105**(4), 043504 (2022). [arXiv:2112.04466](https://arxiv.org/abs/2112.04466)
17. R. Kallosh, A. Linde, BICEP/Keck and cosmological attractors. *J. Cosmol. Astropart. Phys.* **12**, 00812 (2021). [arXiv:2110.10902](https://arxiv.org/abs/2110.10902)
18. Y. Akrami et al., Planck Collaboration, Planck 2018 results. X. Constraints on inflation. *Astron. Astrophys.* **641**, A10 (2020). [arXiv:1807.06211](https://arxiv.org/abs/1807.06211)
19. R. Kallosh, A. Linde, Universality class in conformal inflation. *J. Cosmol. Astropart. Phys.* **07**, 002 (2013). [arXiv:1306.5220](https://arxiv.org/abs/1306.5220)
20. R. Kallosh, A. Linde, Escher in the Sky. *Comptes Rendus Phys.* **16**, 914 (2015). [arXiv:1503.06785](https://arxiv.org/abs/1503.06785)
21. R. Kallosh, A. Linde, Superconformal generalizations of the Starobinsky model. *J. Cosmol. Astropart. Phys.* **06**, 028 (2013). [arXiv:1306.3214](https://arxiv.org/abs/1306.3214)
22. S.V. Ketov, Starobinsky Model in  $N = 2$  supergravity. *Phys. Rev. D* **89**(8), 085042 (2014). [arXiv:1402.0626](https://arxiv.org/abs/1402.0626)
23. A. Linde, Single-field  $\alpha$ -attractors. *J. Cosmol. Astropart. Phys.* **05**, 003 (2015). [arXiv:1504.00663](https://arxiv.org/abs/1504.00663)
24. Y. Aldabergenov, A. Chatrabhuti, H. Isono,  $\alpha$ -Attractors from supersymmetry breaking. *Eur. Phys. J. C* **81**(2), 166 (2021). [arXiv:2009.02203](https://arxiv.org/abs/2009.02203)
25. R. Kallosh, A. Linde, T. Rube, General inflaton potentials in supergravity. *Phys. Rev. D* **83**, 043507 (2011). [arXiv:1011.5945](https://arxiv.org/abs/1011.5945)
26. C. Pallis, N. Toumbas, Starobinsky-type inflation with products of Kähler manifolds. *J. Cosmol. Astropart. Phys.* **05**(05), 015 (2016). [arXiv:1512.05657](https://arxiv.org/abs/1512.05657)
27. C. Pallis, N. Toumbas, Starobinsky inflation: from non-SUSY To SUGRA realizations. *Adv. High Energy Phys.* **2017**, 6759267 (2017). [arXiv:1612.09202](https://arxiv.org/abs/1612.09202)
28. A.A. Starobinsky, A new type of isotropic cosmological models without singularity. *Phys. Lett. B* **91**, 99 (1980)
29. H.E. Haber, *What is the group of conjugate symplectic matrices?* <http://scipp.ucsc.edu/~haber/index.html#sec6>
30. G. Lazarides, C. Pallis, Shift symmetry and higgs inflation in supergravity with observable gravitational waves. *J. High Energy Phys.* **11**, 114 (2015). [arXiv:1508.06682](https://arxiv.org/abs/1508.06682)
31. N. Aghanim et al., Planck Collaboration, Planck 2018 results. VI. Cosmological parameters. *Astron. Astrophys.* **641**, A6 (2020). [arXiv:1807.06209](https://arxiv.org/abs/1807.06209)
32. M.S. Turner, Coherent scalar-field oscillations in an expanding universe. *Phys. Rev. D* **28**, 1243 (1983)
33. J. Martin, C. Ringeval, First CMB constraints on the inflationary reheating temperature. *Phys. Rev. D* **82**, 023511 (2010). [arXiv:1004.5525](https://arxiv.org/abs/1004.5525)
34. J. Ellis, M.A.G. Garcia, D.V. Nanopoulos, K.A. Olive, Calculations of inflaton decays and reheating: with applications to no-scale inflation models. *J. Cosmol. Astropart. Phys.* **07**, 050 (2015). [arXiv:1505.06986](https://arxiv.org/abs/1505.06986)
35. C. Pallis, Gravitational waves,  $\mu$  Term & Leptogenesis from  $B - L$  higgs inflation in supergravity. *Universe* **4**(1), 13 (2018). [arXiv:1710.05759](https://arxiv.org/abs/1710.05759)
36. C. Pallis, Unitarity-safe models of non-minimal inflation in supergravity. *Eur. Phys. J. C* **78**(12), 1014 (2018). [arXiv:1807.01154](https://arxiv.org/abs/1807.01154)
37. C. Pallis, Q. Shafi, Induced-gravity GUT-scale higgs inflation in supergravity. *Eur. Phys. J. C* **78**(6), 523 (2018). [arXiv:1803.00349](https://arxiv.org/abs/1803.00349)
38. Y. Akrami et al., Planck Collaboration, Planck intermediate results. LVII. Joint Planck LFI and HFI data processing. *Astron. Astrophys.* **643**, A42 (2020). [arXiv:2007.04997](https://arxiv.org/abs/2007.04997)
39. P.A.R. Ade et al. [BICEP and Keck Collaboration], Improved constraints on primordial gravitational waves using Planck, WMAP, and BICEP/Keck observations through the 2018 observing season. *Phys. Rev. Lett.* **127**(15), 151301 (2021). [arXiv:2110.00483](https://arxiv.org/abs/2110.00483)
40. M. Tristram et al., Improved limits on the tensor-to-scalar ratio using BICEP and Planck. *Phys. Rev. Lett.* **127**, 151301 (2021). [arXiv:2112.07961](https://arxiv.org/abs/2112.07961)
41. E.D. Stewart, D.H. Lyth, A More accurate analytic calculation of the spectrum of cosmological perturbations produced during inflation. *Phys. Lett. B* **302**, 171 (1993). [arXiv:gr-qc/9302019](https://arxiv.org/abs/gr-qc/9302019)
42. E.W. Kolb, S.L. Vadas, Relating spectral indices to tensor and scalar amplitudes in inflation. *Phys. Rev. D* **50**, 2479 (1994). [arXiv:astro-ph/9403001](https://arxiv.org/abs/astro-ph/9403001)
43. E. Allys et al., [LiteBIRD collaboration], Probing cosmic inflation with the LiteBIRD cosmic microwave background polarization survey. [arXiv:2202.02773](https://arxiv.org/abs/2202.02773)